International Journal of Nanomedicine

Dovepress
Taylor & Francis Group

Open Access Full Text Article

ORIGINAL RESEARCH

Injectable Nanocomposite Hydrogel for Accelerating Diabetic Wound Healing Through Inflammatory Microenvironment Regulation

Yuhui Chen[1,*], Ying Li[1,*], Haoning Song[1,*], Xiaochun Liu[1], Hongan Zhang[1], Jiaxin Jiang[2], Hongsheng Liu[2], Ribo Zhuo[1], Guoyun Cheng[1], Jia Fang[1], Lei Xu[1], Yong Qi[1], Dawei Sun[1]

[1]Department of Orthopedics and Traumatology, The Affiliated Guangdong second Provincial General Hospital of Jinan University, Guangzhou, Guangdong, 510315, People's Republic of China; [2]Guangdong Huayi Biomedical Science and Technology Center, Guangzhou, Guangdong, 511450, People's Republic of China

*These authors contributed equally to this work

Correspondence: Lei Xu, Department of Orthopedics and Traumatology, Guangdong second Provincial General Hospital of Jinan University, No. 466 Xingang Middle Road, Haizhu District, Guangzhou, Guangdong, People's Republic of China, Email orthoxl@163.com; Dawei Sun, Department of Orthopedics and Traumatology, Guangdong second Provincial General Hospital of Jinan University, No. 466 Xingang Middle Road, Haizhu District, Guangzhou, Guangdong, People's Republic of China, Email sundw@gd2h.org.cn

Background: A paramount issue in the realm of chronic wound healing among diabetic patients is the pervasive inflammatory response that persistently thwarts angiogenesis, thereby precipitating protracted delays in the healing process of such wounds. Employing zeolitic imidazolate framework-8 (ZIF-8) as a drug delivery platform, integrated within a temperature-sensitive injectable hydrogel, presents an intriguing strategy for the closure of various irregular wounds, modulation of inflammatory responses, and promotion of angiogenesis.

Methods: Herein, ZIF-8 loaded with curcumin (Cur) combined with methylcellulose/carboxymethyl chitosan (MCC) thermosensitive hydrogel was described. The assessment encompassed the temperature-sensitive properties, pH-responsive release, antimicrobial activity, and ROS scavenging capabilities of the MCC@ZIF-8@Cur hydrogel. A series of studies were conducted to explore its biocompatibility, pro-angiogenic effects, and macrophage M2 polarization induction. Additionally, a full-thickness skin defect model of diabetic rat was established to investigate the hydrogel's multifaceted efficacy in facilitating wound repair, mitigating inflammatory responses, and fostering angiogenesis.

Results: The thermosensitive MCC@ZIF-8@Cur hydrogel possess the attribute of being injectable and capable of in situ formation (gelation temperature of ≥ 28 °C), thereby establishing an effective physical barrier for a multitude of irregular wound profiles. The incorporation of ZIF-8@Cur confers the hydrogel with exceptional antibacterial properties and the capability to eliminate reactive oxygen species (ROS). Moreover, the pH-responsive MCC@ZIF-8@Cur hydrogel continuously releases Cur and Zn^{2+}, mitigating inflammation, inducing M2 polarization of macrophages, and promoting angiogenesis. This creates a favorable immune microenvironment conducive to skin regeneration, thereby accelerating the healing of diabetic wounds. In vivo studies have demonstrated a markedly accelerated wound healing ratio in rats within the hydrogel group compared to the Control group ($p<0.001$). By the 14th day of wound healing, the MCC@ZIF-8@Cur hydrogel group achieved a remarkable healing ratio of 97.22%, considerably surpassing the Control group (72.98%), showcasing remarkable potential for treating diabetic wounds.

Conclusion: The findings demonstrate the successful creation of a temperature-sensitive hydrogel that exhibits remarkable antibacterial properties and ROS scavenging capabilities. This hydrogel effectively suppresses inflammatory responses, modulates the polarization of macrophages towards the M2 phenotype, and promotes angiogenesis, thus fostering a favorable immune microenvironment for skin regeneration. These attributes collectively augur promising prospects and applications in the healing of diabetic wounds.

Keywords: diabetic wound, thermosensitive hydrogel, inflammatory microenvironment, macrophage polarization, angiogenesis

Received: 21 November 2024
Accepted: 21 January 2025
Published: 6 February 2025

Graphical Abstract

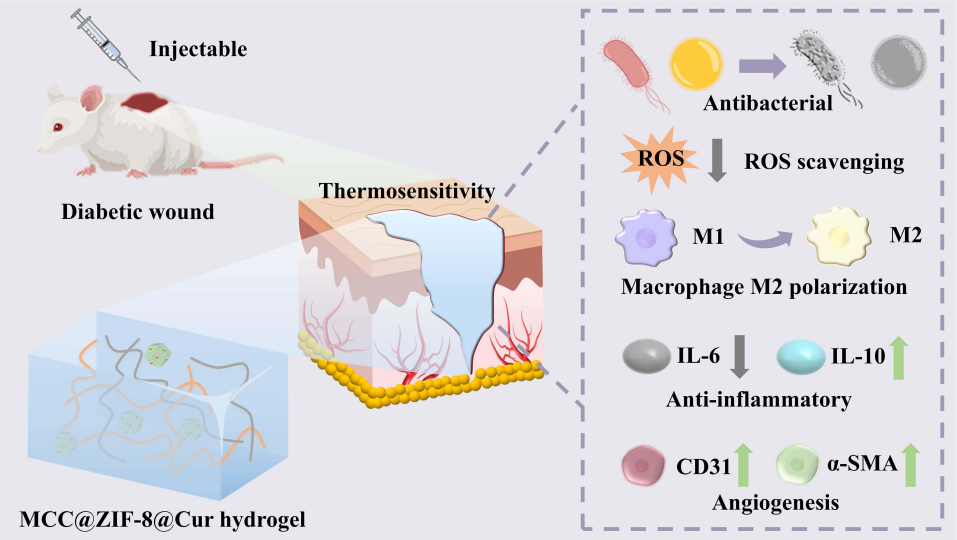

Introduction

Due to the increasing prevalence of an aging population and obesity, the incidence of diabetes mellitus (DM) is rising globally.[1,2] Patients with DM often exhibit delayed wound healing, facing risks of amputation and mortality.[3] In high glucose milieu environment, molecules such as proteins, lipids, and nucleic acids go through non-enzymatic glycation reactions to form advanced glycation end products (AGEs). These AGEs are not only difficult to decompose but also trigger inflammatory responses. Additionally, high blood sugar triggers oxidative stress reactions, producing large amounts of reactive oxygen species (ROS), which can damage cells and tissues, thereby activating inflammatory responses. Inflammatory responses release a plethora of pro-inflammatory cytokines, such as tumor necrosis factor-alpha (TNF-α), interleukin-1 beta (IL-1β), and interleukin-6 (IL-6). These factors inhibit the expression of pro-angiogenic factors, such as vascular endothelial growth factor (VEGF) and fibroblast growth factor (FGF), while also suppressing the proliferation and migration of endothelial cells, thereby impeding angiogenesis.[4–6] Macrophages serve as pivotal regulators in the healing process of DM wounds, transitioning from the inflammatory phase to the subsequent proliferative stage. They can be activated and modulated to various polarized states according to the microenvironment, with M2 macrophages playing an essential role in the reconstruction of wound vasculature.[7,8] However, diabetes impairs the functional responsiveness of macrophages and hinders the phenotypic transition from the inflammatory (M1) to the anti-inflammatory (M2) state.[9] Therefore, developing materials that can regulate macrophage polarization and promote angiogenesis is an innovative therapeutic strategy for chronic DM wounds.[10]

Monomers derived from traditional Chinese herbs are extensively researched in the realm of wound healing, owing to their minimal toxicity and resistance to pharmacological inhibitors, especially those possessing antimicrobial and anti-inflammatory properties.[11,12] Curcumin (Cur), demonstrated to be highly effective in promoting the healing of DM wounds.[13] Ding et al synthesized Zn-Cur nanoparticles endowed with potent antioxidant and anti-inflammatory properties, which facilitate diabetic wound healing by remodeling the immune microenvironment.[14] Li et al harnessed the potential of phenylboronic acid (PBA) to target bacteria, designing PBA-functionalized dextran was developed to encapsulate Cur that exhibit remarkable antibacterial efficacy, significantly promoting the healing of bacterially infected diabetic wounds.[15] However, Cur has low bioavailability due to its hydrophobicity, loading Cur into nanoparticles represents an effective strategy to enhance its bioavailability.[16,17] Metal-organic frameworks (MOFs), a new class of porous hybrid materials, are composed of inorganic metal centers and organic ligands, it can be used as a delivery system

for Cur due to their high specific surface area and porosity.[18,19] Among these, Zeolitic Imidazolate Framework-8 (ZIF-8) demonstrates excellent antimicrobial properties, biocompatibility, and pH-responsiveness, and can facilitate angiogenesis.[20,21] Li et al[22] employed ZIF-8 for the delivery of BMP-2 to accelerate vascularized bone regeneration, proving that ZIF-8 can increase the expression of fibroblast growth factor (FGF) and vascular endothelial growth factor (VEGF) to encourage vascular regeneration. Guo et al[23] applied ZIF-8 to chronic wound healing in diabetes, confirming its remarkable antimicrobial properties. By alleviating mitochondrial dysfunction and endoplasmic reticulum stress, the hydrogel fundamentally improves high glucose-induced cellular damage, endows ROS scavenging and anti-apoptotic activities, and promotes endothelial cell migration, thereby achieving excellent vascular regeneration.

However, ZIF-8 suffers from limitations such as poor dispersion and susceptibility to degradation.[24,25] Instead of using ZIF-8 directly as a drug delivery system, incorporating it into hydrogels can perform its exceptional functional properties. The functional groups within the hydrogel matrix can chelate with metal ions, enhancing dispersion and controlled release, while also improving the mechanical properties of the hydrogel.[26–28] Injectable hydrogels possess the remarkable property of in situ formation, enabling seamless filling of defects, thereby holding significant potential in wound repair applications. Wang et al have developed an injectable dual-network hydrogel based on gelatin methacrylate (GelMA) and oxidized hyaluronic acid (OHA), utilizing Schiff base reactions and UV light-initiated free radical polymerization for in situ gelation, offering a promising option for corneal repair and regeneration.[29] Zhang et al have developed an injectable double network hydrogel comprised of a catechol-branched polyacrylamide network created through radical polymerization and a chitosan-oxidized hyaluronic acid covalent network formed via Schiff base condensation, achieving efficient and immediate wound hemostasis and sealing.[30] However, chemical reactions such as Schiff base condensation and radical polymerization can irritate the wound, potentially causing additional harm. Thus, the gentle gelation conditions of temperature-sensitive hydrogels make them more suitable for wound application scenarios. Most temperature-sensitive hydrogels exhibit a sol state at elevated temperatures, transitioning into a gel state upon cooling, such as Gellan Gum and Poloxamer 407.[31] However, the suboptimal injectability of these temperature-responsive hydrogels, coupled with their elevated storage costs and challenges in loading active components (which are prone to deactivation at high temperatures), significantly hampers their applicability in wound management scenarios. In contrast, methylcellulose (MC) exhibit a robust flowability at low temperatures and undergo gelation as the temperature rises when injection onto the wound surface. Its exceptional injectability and the mild conditions required for gelling hold significant promise as a sophisticated, intelligent material for efficient wound healing.[32,33]

In this study, we present a MC/carboxymethyl chitosan (CMC) double-network hydrogel (MCC hydrogel) that incorporates in situ synthesized Curcumin-loaded ZIF-8 (ZIF-8@Cur). This hydrogel demonstrates resistance to bacterial infections, ROS scavenging, reduction in inflammatory symptoms, promotion of angiogenesis, and improvement in DM wound healing. Under the regulation of hydrogen bonding interactions between dual networks and the metal coordination of ZIF-8@Cur nanoparticles, MCC@ZIF-8@Cur hydrogels can undergo sol-gel phase transitions at human body temperature, which is conducive to close various irregular wounds. Cur, assisted by the ZIF-8 system, shows exceptional ROS scavenging activity and pH-responsive drug release in the acidic wound environment. The MCC enhances the stability of ZIF-8@Cur and the sustained release of Zn^{2+}, continually promoting angiogenesis. Designed to address the specific characteristics of DM wounds, this hydrogel utilizes the modulation of macrophage M2 polarization to alleviate the inflammatory response, accelerates angiogenesis, and thus provides a novel strategy for treating diabetes-related wounds (Figure 1).

Methods

Materials

2-Methylimidazole (98%), curcumin (98%), carboxymethyl chitosan and methanol (99.5%) were acquired from Shanghai Macklin Biochemical Technology Co., Ltd. $Zn(NO_3)_2{\cdot}6H_2O$ (99%) and Methyl Cellulose (15 mPa·s, M_n=454.5) were purchased from Shanghai Aladdin Biochemical Technology Co., Ltd.

https://doi.org/10.2147/IJN.S505918

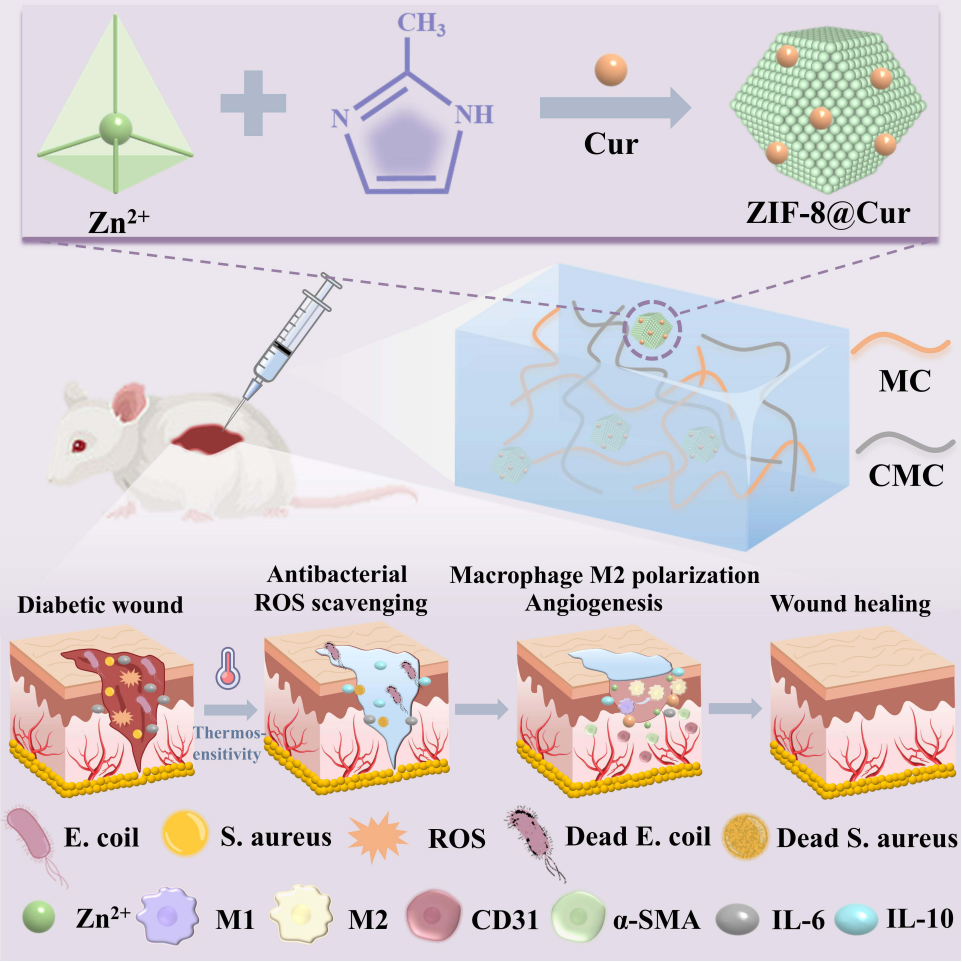

Figure 1 Schematic illustration of preparation and application in diabetic wound healing of the MCC@ZIF-8@Cur hydrogel.

Synthesis of ZIF-8@Cur Nanoparticles

2-Methylimidazole (2.5 g, 61 mmol) and Cur (15 mg, 0.05 mmol) were completely dissolved in a methanol solution (25 mL). Dissolve $Zn(NO_3)_2{\cdot}6H_2O$ (0.25 g, 0.83 mmol) in 5 mL methanol solution, and add it to the above solution by drops, stir at room temperature for 12 h.[34] The resulting precipitate was washed with methanol at 12,000 rpm three times for 15 min. ZIF-8@Cur nanoparticles were obtained and collected by freeze-drying. Similarly, ZIF-8 nanoparticles can be prepared. X-ray diffraction (XRD) analysis of the nanoparticles was conducted using an X-ray diffractometer (Rigaku-SmartLab, Japan). in addition, a transmission electron microscope (TEM, JEOL F200, USA) was used to investigate the morphology of ZIF-8@Cur and ZIF-8 nanoparticles.

Synthesis of MCC@ZIF-8@Cur Hydrogel

The 10 wt% MC aqueous solution was stirred at 70 °C for 30 minutes and left at room temperature for 1 h, then refrigerated for one day. After that, 0.1 mol of $Zn(NO_3)_2{\cdot}6H_2O$, carboxymethyl chitosan (CMC, 4 wt%) and ZIF-8@Cur (0.4 wt%) were added to the MC solution in the ice bath under magnetic rotation. Place the mixed solution in a water bath at 37 °C, allowing the sol to undergo a transformation into a gel, hereby designated as the MCC@ZIF-8@Cur hydrogel. The hydrogels' microstructure was examined using a scanning electron microscope (SEM, Sigma300, Zeiss, Germany).

Characterization

Rheological Property of Hydrogels

The rheometer (DHR, TA Instruments, USA) was used to measure the phase transition temperatures and viscosities of hydrogels under temperature scanning circumstances with a frequency of 6.28 rad/s and a constant oscillatory strain of 1%.

Swelling and Release of Simulated Drug

The freeze-dried hydrogels were immersed in phosphate buffered brine (PBS, 0.1 M, pH 7.4), and their swelling properties were assessed at 37 °C. The swelling ratio was calculated by Eq (1):

$$Swelling\,ratio(\%) = \frac{W_t - W_i}{W_i} \times 100\% \tag{1}$$

Where, the W_i is initial mass of freeze-dried hydrogel and W_t is the mass of hydrogel after swelling at different time (The unit of W_i and W_t is g).

The Cur release experiment: The MCC@ZIF-8@Cur hydrogel was placed in a dialysis bag (Mw = 20,000 Da) and submerged in PBS solutions with pH values of 5.2 and 7.1. Incubation was conducted in a shaker at 37 °C. At designated time intervals, the absorbance of the solution at 420 nm was measured using a UV spectrophotometer. The release amount of Cur in different pH solutions was calculated with the aid of a Cur standard curve.

The mathematical fitting method was used to assess the kinetics of Cur release.

Zero-order release:

$$Q = Kt + Q_0 \tag{2}$$

First-order release:

$$In(1 - Q) = -Kt \tag{3}$$

Higuchi:

$$Q = Kt^{\frac{1}{2}} \tag{4}$$

Korsmeyer-Peppas:

$$Q = Kt^n \tag{5}$$

In this context, K represents the ratio constant of release, n denotes the diffusion exponent of the drug release mechanism, and Q signifies the amount of drug released at a specified time.

Antibacterial and Antioxidant Experiment

A turbidimetry methodology and the spread plate method were used to evaluate the antibacterial efficacies of various formulations against *Staphylococcus aureus* (*S. aureus*) and *Escherichia coli* (*E. coli*). The PBS, MCC and MCC@ZIF-8@Cur hydrogels were co-cultured with bacterial suspension (100 μL, 1×10^6 CFU/mL) and 900 μL agar-protein medium, respectively. Subsequently, OD value of bacterial suspension at a wavelength of 570 nm was measured by microplate reader (Biotek Synergy H1). In the meantime. To further confirm the antibacterial capability of hydrogels, 100 μL bacterial suspension cultured with different groups of hydrogels for 6 h was diluted 10^6-fold with PBS, and then 100 μL diluted bacterial suspension was coated in LB AGAR plate, incubated for 12 h, optical imaging was conducted. In addition, in order to verify the release of Zn^{2+} by cleavage of ZIF-8, the co-culture time was extended to 12 h when the antibacterial activity of ZIF-8 group and ZIF-8@Cur group was compared. Using Eq (6), the bacterial survival ratio was determined.

$$Bacterial\,survival\,ratio\ (\%) = \frac{N_{hydrogel}}{N_{blank}} \times 100\% \tag{6}$$

N_{blank} and N_{hydrogel} represent the bacterial counts of the blank group and the hydrogel group, respectively.

https://doi.org/10.2147/IJN.S505918

Using DPPH free radical kit, the samples' antioxidant capacity was assessed. A UV-Visible spectrophotometer (Shimadzu UV-3600 plus, Japan) was employed to assess the absorbance at a wavelength of 517 nm. Using Eq (7), the DPPH-scavenging activity was determined.

$$DPPH\ scavening\ activity\,\% = \left(1 - \frac{A_s}{A_c}\right) \times 100\% \tag{7}$$

Where A_s and A_c denote the absorbance values of the sample and the control at a wavelength of 517 nm, respectively.

Cytotoxicity Evaluation of Hydrogels

CCK-8 Assay and Live/Dead Staining

Human umbilical vein endothelial cells (HUVECs), procured from Wuhan Procell Life Technology Co., Ltd., were employed to evaluate the biocompatibility of hydrogels. First, HUVECs were seeded onto aseptic hydrogel surfaces at a density of 1×10^4 cells per well. Subsequently, the cells were cultured for 1, 3, and 5 days, during which time their proliferation and viability on the hydrogel were assessed through live/dead co-staining assays and CCK-8 assays, respectively.[35]

Cytoskeleton Staining

To evaluate the expanding shape and cell spreading of HUVECs upon adhesion to the hydrogel, after co-culturing HUVECs with hydrogels of various components for three days, cells were subjected to immunostaining using rhodamine-conjugated phalloidin to visualize the F-actin filaments, alongside 4′, 6-diamidino-2-phenylindole (DAPI, Life) for the nuclear component. This was done in the dark, and the results were observed using confocal laser scanning microscopy (LSM, leica stellaris5, Zeiss, Germany).[36]

Characterization of the Antioxidant Capacity of Hydrogels Extracellularly

An oxidative stress cell model was established using H_2O_2 to stimulate the generation of ROS in HUVECs cells. Briefly, HUVECs were inoculated into 12-well plates (5×10^4 cells/well) and cultured overnight to allow cell adhesion. H_2O_2 (400 μM) and different preparations were added and incubated for 2 h. After that, 10 μM 2', 7'-dichlorofluorescein diacetate (DCFH-DA) was used to stain HUVECs for 30 minutes, then observed using an inverted fluorescent microscope (Leica, DMi8-s).

Cell Migration Experiment

In a fully confluent HUVECs, vertical scratches were made by sterile 200 μL pipette tip. Subsequently, the scratch areas were treated with PBS, MCC, and MCC@ZIF-8@Cur hydrogel extracts, respectively, and imaged at 0 h and 24 h.[37] Using Image J software, the changes in the wound region were measured. Eq (8) was used to calculate the migration ratio.

$$Migration\ ratio\ (\%) = \frac{W_0 - W_{24}}{W_0} \times 100\% \tag{8}$$

Where W_0 and W_{24} represent the wound areas at 0 and 24 hours, respectively.

Tube Formation Assay

The impact of MCC@ZIF-8@Cur hydrogel on tube formation was evaluated using Matrigel. Prior to adding HUVECs (5000 pieces/well), 96-well plates were coated with Matrigel (50 μL/well) and allowed to cure for 30 minutes at 37 °C. After 1–2 hours, the supernatant was discarded, and HUVECs was cultivated for 10 hours in a new serum-free medium with PBS, MCC, and MCC@ZIF-8@Cur hydrogel extracts, respectively. The creation of tubes were then observed.[38]

Experiment on Macrophage Polarization

To demonstrate the ability of hydrogels to induce macrophage polarization, mouse monocytic macrophage leukaemia cells (RAW264.7) were first inoculated into 6-well plates and treated with 10 ug/mL LPS for 48 h to induce macrophage polarization towards a pro-inflammatory phenotype (M1) and different preparations were added and incubated for 48 h.

Next, macrophages were subjected to fixation, permeabilization, and blocking with 4% paraformaldehyde, 0.5% Triton, and 10% BSA. An analysis of immunofluorescence staining was subsequently conducted: in short, cells were incubated overnight at 4 °C with primary antibodies targeting CD86 (a marker for M1 macrophages) or CD206 (a marker for M2 macrophages), followed by a 30-minute incubation with the respective fluorescence-labeled secondary antibodies. Finally, following DAPI staining of the cell nuclei, the samples were seen using a fluorescence microscope.[39]

In vivo Animal Experiment

Sprague-Dawley (SD) rats, with weights ranging from approximately 220 to 250 g, were employed in the experiment. All animal experiments were approved by the Experimental Animal Ethics Committee of Guangdong Second People's Hospital (2024-DW-SB-33) and carried out in accordance with the National Institutes of Health's guidelines for the care and use of laboratory animals. First, after 2 weeks of feeding on a high-fat, high-sugar diet, a tool was used to create a circular wound with a diameter of 20 mm, and the wound was treated with PBS, MCC and MCC@ZIF-8@Cur hydrogel. Wound closure was observed on days 1, 3, 5, 7, 9, and 14, and the ratio of wound healing was evaluated using Image J software. The rats were put to death on the fourteenth. Subsequently, the lesions together with their surrounding tissues were taken out for histological assessment using conventional techniques. This included Hematoxylin & Eosin (H&E), Masson staining, interleukin-10 (IL-10), interleukin-6 (IL-6), α-SMA, and CD31 immunofluorescence.

Statistical Analysis

All experimental results are reported as mean ± S.D. unless otherwise noted. Every experiment was run through three replications, and the ANOVA/Tukey's test was statistically analyzed using SPSS 27.0. The following values were regarded as indicating statistically significant differences: $*p<0.05$, $**p<0.01$, and $***p<0.001$.

Results and Discussion

Synthesis and Characterization of ZIF-8@Cur Nanoparticles Modified Temperature-Sensitive MCC Hydrogel

ZIF-8@Cur nanoparticles were synthesized via a simple one-pot method, where Zn^{2+} and 2-methylimidazole self-assembled in the presence of in situ curcumin doping. Figure 2a illustrates that the XRD spectrum reveals the crystal structure of ZIF-8 remains unaffected by the incorporation of Cur, with the nanoparticle size consistently around 200 nm (Figure 2b). The color change observed in the nanoparticles as depicted in the real image of Figure 2c confirms the successful loading of Cur. Overall, the porous structure based on MOF effectively encapsulates Cur in situ within ZIF-8 during synthesis, while preserving the stability and particle size of ZIF-8.

Thermoresponsive hydrogels within the physiological temperature range can profoundly fill irregular wounds. Due to its rich hydrophobic methoxy groups, MC exhibits unique thermal gel properties through the hydrophobic force between molecules, and transforms from solution to gel with increasing temperature. In order to reduce the gelling temperature of the MC hydrogel, CMC is introduced into the MC hydrogel to construct a hydrogen interlocked MCC double crosslinked hydrogel. Meanwhile, nanoparticles are infused with ZIF-8@Cur to enrich the metal coordination bond interaction of the hydrogel network. As depicted in Figure 2d, the gelation process of the MC, MCC and MCC@ZIF-8@Cur hydrogels can be observed, with gelation time calculated in Figure 2e. The incorporation of CMC enhances the interactions within the hydrogel, facilitating the self-assembly of MC molecular chains into a fibrillar structure during the heating process, thereby reducing the gelation time. Furthermore, the strong metal chelation between ZIF-8@Cur nanoparticles and MCC significantly shortens the gelation time of the hydrogel to 475 s. The specific temperature of gelation was determined through rheology, as illustrated in Figure 2f. The intersection of the storage modulus (G') and the loss modulus (G") represents the sol-gel transition of the hydrogel. The phase transition temperature of MCC hydrogel is approximately 38 °C, whereas the gelation temperature of MCC@ZIF-8@Cur is reduced to 28 °C. The gelation temperature based on the research on MC temperature-sensitive hydrogels is listed and compared (Table S1). The hydrogen bond interaction with macromolecular polymers and the coordination of metal ions are the main strategies to regulate the gelation temperature of MC hydrogels. We found that according to the application environment of human body, most studies would regulate

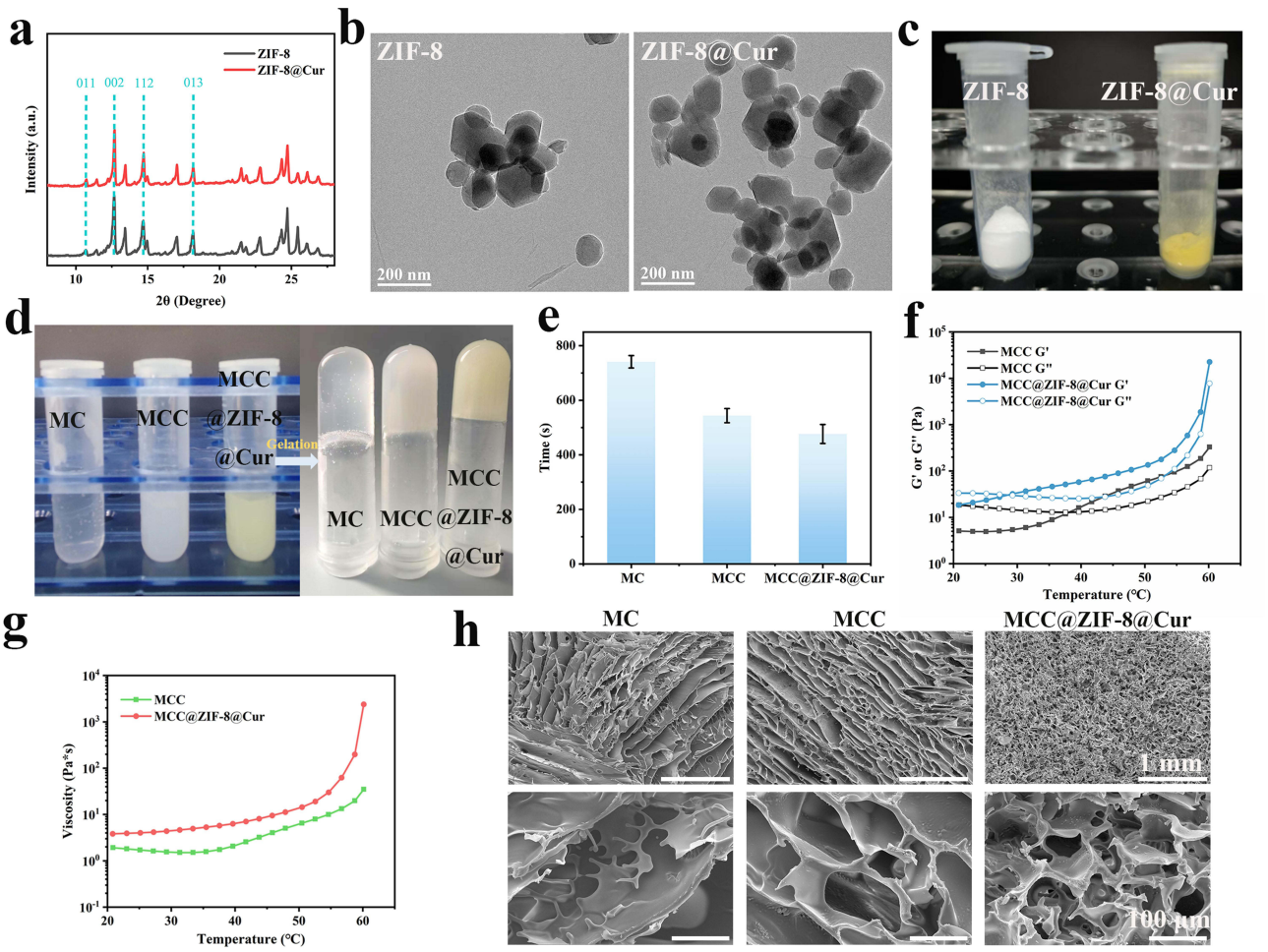

Figure 2 (**a**) XRD spectrum of nanoparticles. (**b**) TEM images of nanoparticles. (**c**) Macroscopic picture of nanoparticles. (**d**) Sol–gel phase transition of hydrogels. (**e**) Gelation time of different groups of hydrogels. (**f**) The modulus of hydrogel was measured by dynamic temperature scanning. (**g**) Viscosity-temperature curve of hydrogels. (**h**) SEM images of the hydrogels.

the temperature of hydrogels below 37 °C as far as possible. In order to achieve the injectivity of hydrogels at room temperature, Therefore, it is a suitable temperature to control the gelation temperature of MCC@ZIF-8@Cur hydrogel above 28 °C. Subsequently, the viscosity of MCC and MCC@ZIF-8@Cur hydrogel was tested (Figure 2g), as the temperature increased, the viscosity of the hydrogel progressively rose, the thermosensitive gelation property of MCC@ZIF-8@Cur hydrogel was confirmed. Furthermore, MCC@ZIF-8@Cur hydrogel exhibits enhanced viscosity, demonstrating that ZIF-8@Cur nanoparticles increasing the cross-linking of the hydrogel network, facilitating gelation, and improving mechanical performance. SEM observations of the lyophilized hydrogel's morphology reveal that the structural cross-linking of MCC double-network hydrogel is significantly increased, MCC@ZIF-8@Cur hydrogel exhibit rich, uniform, and dense porous structure (Figure 2h). The pore size of MC hydrogel is 201.80±26.79 nm, reducing to 116.26±10.85 nm in MCC hydrogel, and the pore size of MCC@ZIF-8@Cur hydrogel is diminished to an even smaller size of 74.78±11.03 nm (Figure S1). In summary, the MCC@ZIF-8@Cur hydrogel remains in solution at low temperatures and can be applied to wounds via injection, accommodating various irregular and deep wounds, while rapidly gelling at body temperature to form an effective physical barrier.

Swelling and Release of Simulated Drug of Hydrogels

The swelling properties of hydrogels play a crucial role in the absorption of wound exudates. As illustrated in Figure 3a, compared to MC and MCC hydrogels, the swelling ratio of MCC@ZIF-8@Cur hydrogel decreases, which is

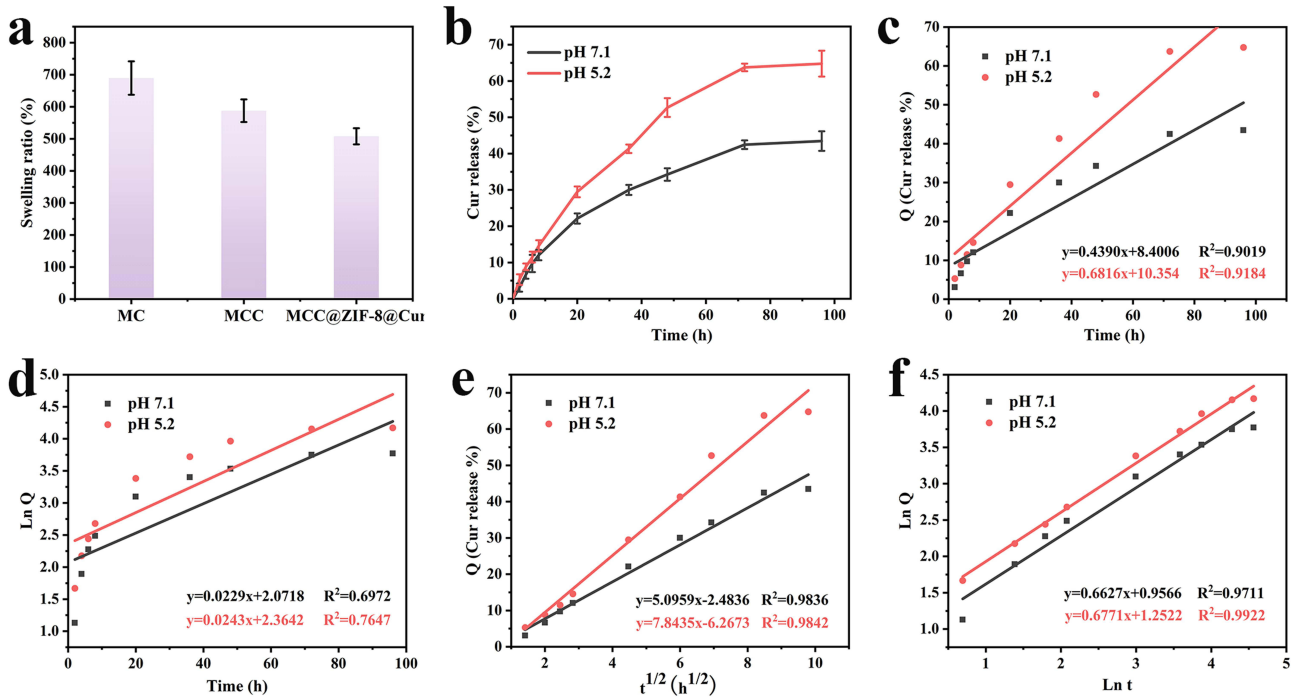

Figure 3 (**a**) Hydrogels' swelling ratio in PBS after 24 hours. (**b**) Drug release curves of MCC@ZIF-8@Cur hydrogels in PBS at different pH. (**c**) Zero-order simulation, (**d**) First-order simulation, (**e**) Higuchi simulation and (**f**) Korsmeyer-Peppas simulation of drug release from MCC@ZIF-8@Cur hydrogels in PBS at different pH.

advantageous for maintaining the mechanical properties of the hydrogel while still achieving approximately 550% swelling. Drug release was examined in PBS solutions at pH 7.1 and 5.2 to mimic circumstances found in human DM wounds. Figure 3b clearly shows that in an environment with pH 5.2, the ZIF-8 framework is more prone to degradation, leading to a significant acceleration in Cur release.[40] In order to more thoroughly assess the kinetics and mechanism of Cur release from MCC@ZIF-8@Cur hydrogel, zero-order, first-order kinetic, Higuchi and Korsmeyer-Peppas models were used to evaluate the release.[41] Based on the fitted curves (Figure 3c–f), a comparison of the R^2 values of Cur's release in acidic and neutral environments. The Higuchi model exhibits a higher R^2 than the other models at pH 7.1, which is employed to investigate the drug diffusion-controlled release, this implies that Cur is released from the MCC@ZIF-8@Cur hydrogel primarily by diffusion mechanisms at pH 7.1. Nonetheless, the Korsmeyer-Peppas model yields the closest R^2 to 1 in the acidic pH 5.2 environment, this model is commonly used for analyzing release mechanisms that are not well-defined or involve multiple concurrent release phenomena. It is suggesting that the release of Cur is controlled by various release mechanisms at pH 5.2. Where $n = 0.6771$, and thus $n > 0.5$ (n represents the slope value in the Korsmeyer-Peppas equation for modeling), is the non-Fickian release. This implies that drug release may be influenced by both diffusion and polymer swelling. In conclusion, the model fitting proved that the release behavior of Cur in MCC@ZIF-8@Cur hydrogel was affected by the pH of the environment, and the phenomenon that Cur was released faster in acidic environment was confirmed. The MCC@ZIF-8@Cur hydrogel could adjust and control the release of Cur based on wound pH fluctuations when applied, so as to achieve the pH response release effect. In DM wounds, the accumulation of acidic metabolites leads to a decrease in the pH value of the wound microenvironment. The ZIF-8@Cur within the MCC@ZIF-8@Cur hydrogel rapidly disintegrates under acidic conditions, thereby accelerating the release ratio of Cur. As the microenvironment stabilizes and the pH gradually normalizes, the precise release of Cur effectively promotes wound healing.

Antioxidant Ability and Antibacterial Activities and of Hydrogels

ROS exacerbate the damage and healing difficulties of DM wounds. Antioxidant hydrogels can mitigate the harm caused by ROS and promote wound healing.[42] The DPPH radical scavenging assay is an effective method for evaluating the in

https://doi.org/10.2147/IJN.S505918

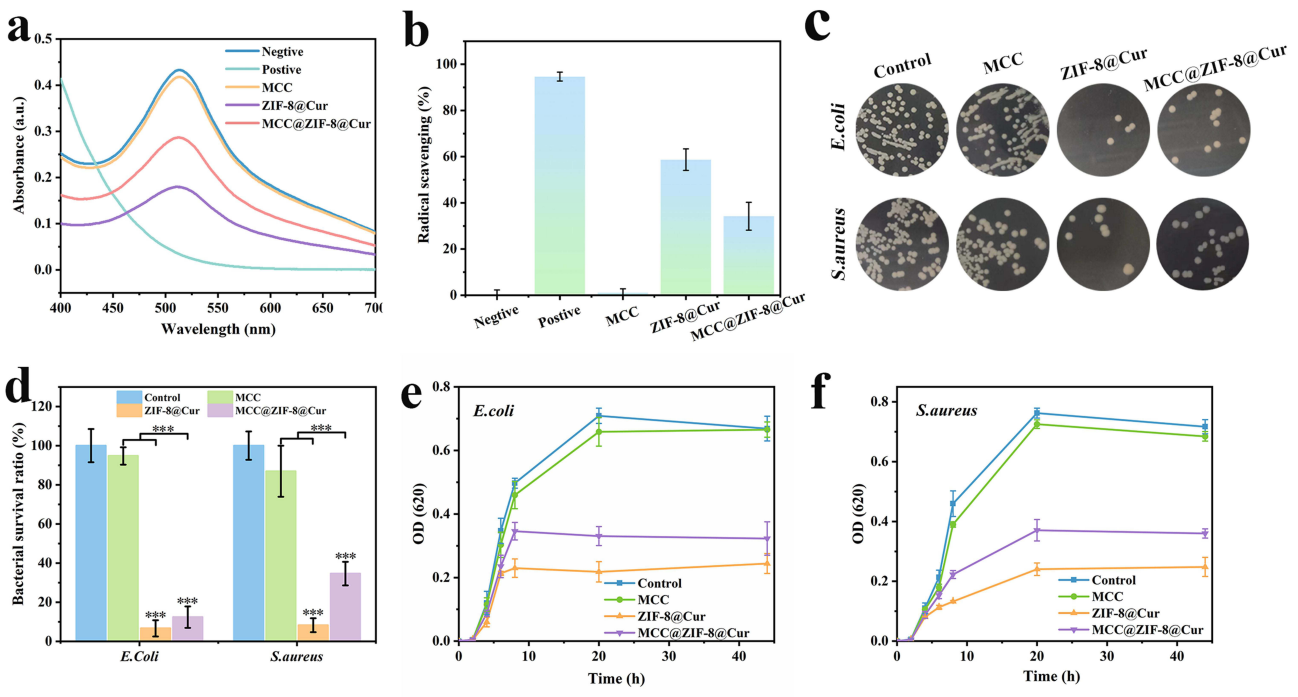

Figure 4 (**a**) UV absorption curves of DPPH after treatment with hydrogels. (**b**) Radical scavenging abilities of hydrogels. (**c**) Optical images of *E. coli* and *S. aureus* colonies after 6 h of co-culture with hydrogels. (**d**) Bacterial survival ratio of *E. coli* and *S. aureus* after 6 h of co-culture with hydrogels. (**e**) Growth curves of *E. coli* and (**f**) *S. aureus* co-cultured with hydrogels. Significance levels of ***$p<0.001$ were applied.

vitro radical scavenging capacity of antioxidant drugs. It can be seen from Figure 4a that the absorbance of the hydrogel treatment group at 517 nm showed a regular decline. The radical scavenging ratio of the various components can be calculated based on the peak intensities (Figure 4b). The results showed that the components loaded with Cur had obvious antioxidant effect, compared to the 34.28% radical scavenging ratio of MCC@ZIF-8@Cur hydrogel, ZIF-8@Cur nanoparticles alone exhibit a higher radical scavenging ratio of 58.83%, indicating that the hydrogel encapsulates and releases the nanoparticles more gradually.

Diabetes-related chronic wounds are more prone to bacterial infections.[43] To examine the antibacterial efficiency of hydrogels, typical pathogens for Gram-positive and Gram-negative bacterial infections, respectively, were chosen to be *E. coli* and *S. aureus*. According to Figure 4c, after co-culturing various component materials with bacteria for 6 hours, plate spreading was performed, and the number of colonies was quantified to determine bacterial survival ratio (Figure 4d). Additionally, the optical density (OD) values of *E. coli* and *S. aureus* co-cultured with different materials over time were measured using the turbidity method to record bacterial growth curves (Figure 4e and f). Overall, Strong antibacterial activity is shown by the ZIF-8@Cur nanoparticles containing component against both Gram-positive and Gram-negative bacteria, and obvious antibacterial effect appeared after co-culture for 6 h, indicating that the material has universal antibacterial activity, and the hydrogel has a slow-release effect on the nanoparticles, so as to achieve sustained antibacterial effect. The superior antibacterial performance of ZIF-8@Cur nanoparticles is attributed to the presence of Zn^{2+} and Cur. In addition, it can be clearly observed from the colony images of ZIF-8 group and ZIF-8@Cur group (Figure S2), The ZIF-8@Cur group showed superior antimicrobial properties compared to ZIF-8 alone, which proves that Zn^{2+} and Cur have synergistic antibacterial ability. Zn^{2+} can penetrate bacterial cell membranes, altering membrane permeability and leading to cytoplasmic leakage, thereby killing the bacteria.[44] Cur inhibits bacterial growth by disrupting membrane structures, interfering with bacterial metabolism, and suppressing the production of bacterial toxins.[13]

Cytotoxicity Evaluation and ROS-Scavenging of Hydrogels

Hydrogels with excellent biocompatibility enhance wound healing. The hydrogels' biocompatibility was verified by live (green staining) and dead (red staining) cell assays, as seen in Figure 5a. Various hydrogel compositions were cultured

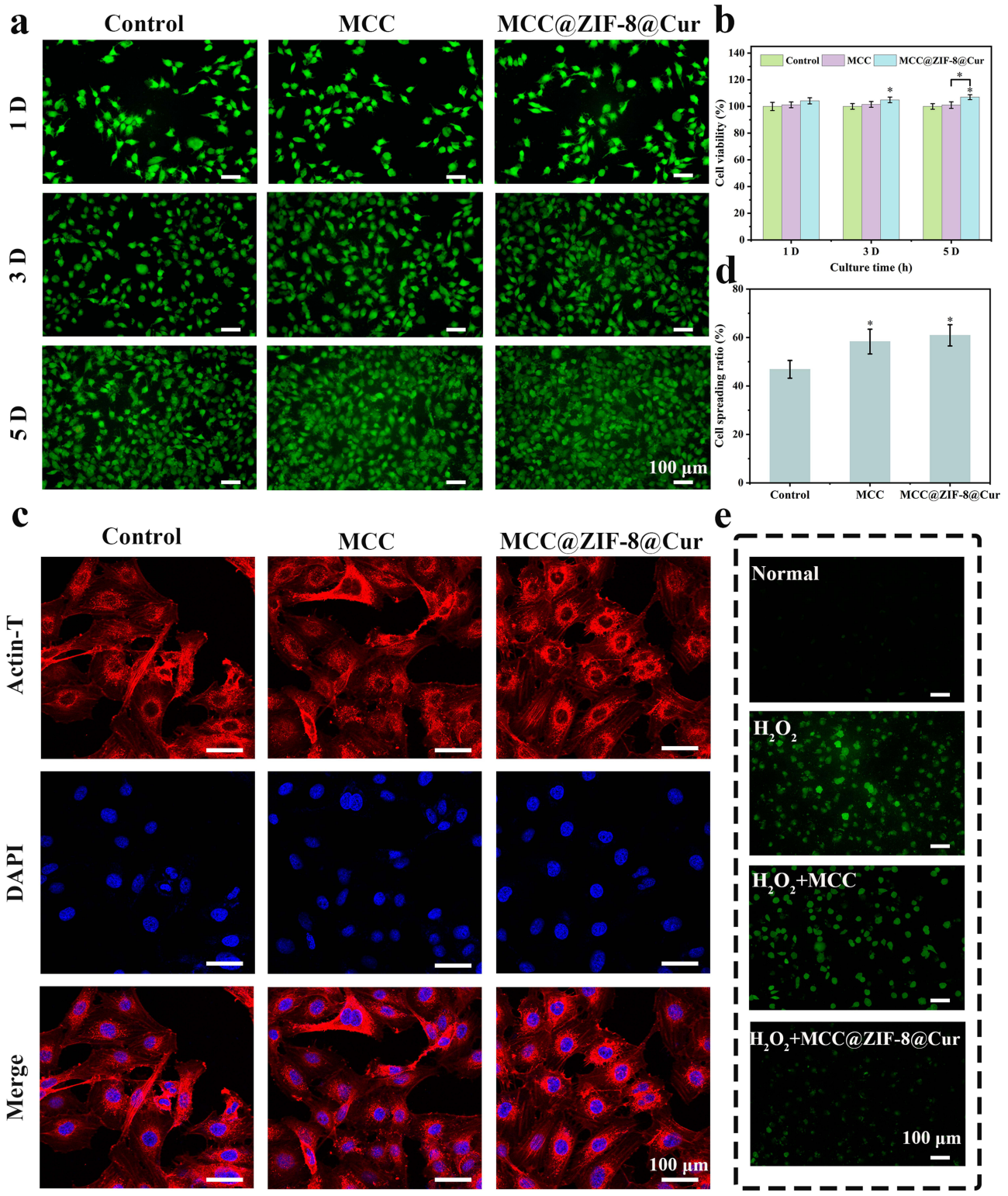

Figure 5 (**a**) Staining of live and dead cells. (**b**) CCK8 assay used to measure cell viability in various groups at 1, 3, and 5 days. (**c**) Images of the cytoskeleton morphology from CLSM. (**d**) Quantitative statistical analysis of the ratio of cell spreading across various hydrogel groupings. (**e**) DCF fluorescence staining of ROS in HUVECs. Significance levels of *$p<0.05$ were applied.

with HUVECs for 1, 3, and 5 days, followed by quantitative analysis (Figure 5b). Taking the cell viability of the Control group at the same time as the baseline, the MCC@ZIF-8@Cur hydrogel group demonstrated superior cell proliferation, with cell viability reaching 110% on the fifth day. This indicates that both MC and CMC, as natural materials, possess

https://doi.org/10.2147/IJN.S505918

outstanding biocompatibility, and MCC@ZIF-8@Cur hydrogel group facilitates cell proliferation, this shows that ZIF-8@Cur nanoparticles exhibited no toxicity. The cytoskeleton regulates cell shape, mechanical characteristics, and signal transduction, all of which are essential for the differentiation and maturation of keratinocytes. Rhodamine-phalloidin (red staining) was used to stain the cytoskeleton of HUVECs, allowing observation of cell morphology and quantitative analysis of cell spreading. As shown in Figure 5c and d, the MCC@ZIF-8@Cur hydrogel group exhibited a larger spreading area with well-defined contours, elongated spindle shape, and clear pseudopodia, indicating that cells on the MCC@ZIF-8@Cur hydrogel can extend and adhere effectively. Therefore, the MCC@ZIF-8@Cur hydrogel demonstrates excellent biocompatibility, promotes cell proliferation, and optimizes the cytoskeleton.

ROS are natural byproducts of oxygen metabolism and accumulate excessively within cells under high glucose stimulation, causing DNA damage, affecting cellular function, and impeding wound healing.[45] As shown in Figure 5e, stimulation of cells with H_2O_2 leads to an overproduction of ROS, and exhibits strong fluorescence. With the intervention of MCC@ZIF-8@Cur hydrogel, the expression of H_2O_2 and fluorescence intensity decreased significantly (Figure S3). As a carrier for Cur, the MCC@ZIF-8@Cur hydrogel can release Cur and continue to have good ROS scavenging action inside of cells, according to the results.

Angiogenesis Analysis and Promoted Macrophage Polarization in Vitro

Vascular dysfunction is a major contributing factor to the poor healing of DM wounds when hyperglycemia is stimulated.[46] To mimic the angiogenesis process of HUVECs and examine the impact of different hydrogel systems on angiogenesis, in vitro research used cell migration and endothelial tube formation assays. As shown in Figure 6a, after 24 hours, the number of migrating HUVECs in the MCC@ZIF-8@Cur hydrogel group significantly increased compared to the Control group and the MCC hydrogel group. Based on a quantitative examination of migration ratio (Figure 6b), the MCC@ZIF-8@Cur hydrogel group migrated ratio is 70.36%, significantly greater than both the MCC hydrogel group (34.55%) and the Control group (28%), highlighting the promoting effect of ZIF-8@Cur nanoparticles on cell migration. Angiogenesis-related metrics all increased in the MCC@ZIF-8@Cur hydrogel group, according to the tube formation test, which is depicted in Figure 6c, d, S4, and S5. This indicates that ZIF-8@Cur nanoparticles play a crucial role in enhancing angiogenesis. This effect is attributed to Zn^{2+}, an essential trace element with significant biological functions in maintaining venous network integrity and hematopoiesis.[46] Zn^{2+} is slowly released from the hydrogel encapsulation, promoting angiogenesis continuously without the toxicity that comes with large doses. Additionally, Cur effectively scavenges excess ROS, mitigating oxidative damage and further promoting angiogenesis.

The induced effect of hydrogel on macrophage polarization was investigated by immunofluorescence staining. M1 phenotype macrophages play a leading pro-inflammatory role in immune regulation, while M2 phenotype macrophages exert an anti-inflammatory effect. Lipopolysaccharide (LPS) was first employed to induce polarization of RAW264.7 macrophages towards the M1 phenotype. Subsequently, different hydrogel compositions were co-cultured with the cells for 48 hours. CD86 and CD206 were used as markers of M1 phenotype and M2 type macrophages, respectively. The results revealed that compared to the Control group and MCC hydrogel group, the weak expression of CD86 (green fluorescence) and strong expression of CD206 (red fluorescence) were significantly observed in the MCC@ZIF-8@Cur hydrogel group (Figure 6e). This suggests that MCC@ZIF-8@Cur hydrogel can stimulate macrophage polarization towards the M2 phenotype, suppress the production of inflammatory mediators, alleviate inflammatory responses. In summary, the MCC@ZIF-8@Cur hydrogel can remove excess ROS from cells, induce macrophage M2 polarization modulate the wound immune microenvironment, accelerating angiogenesis and wound healing.

Healing of a DM Wound Defect in a Full-Thickness Model

In order to evaluate the therapeutic effectiveness of hydrogels on DM wounds and create a full-thickness wound defect model, we utilized DM rats as our experimental subjects.[47] As illustrated in Figure 7a, wound healing was observed at 1, 3, 5, 7, 9, and 14 days. In comparison to both the MCC hydrogel group and the Control group, the MCC@ZIF-8@Cur hydrogel group showed a noticeably faster ratio of wound healing. After 14 days, the wounds in the MCC@ZIF-8@Cur hydrogel group had nearly healed, whereas open wounds were still observed in the other two groups. Quantitative analysis based on wound area (Figure 7b) revealed that the MCC@ZIF-8@Cur hydrogel achieved a wound healing ratio

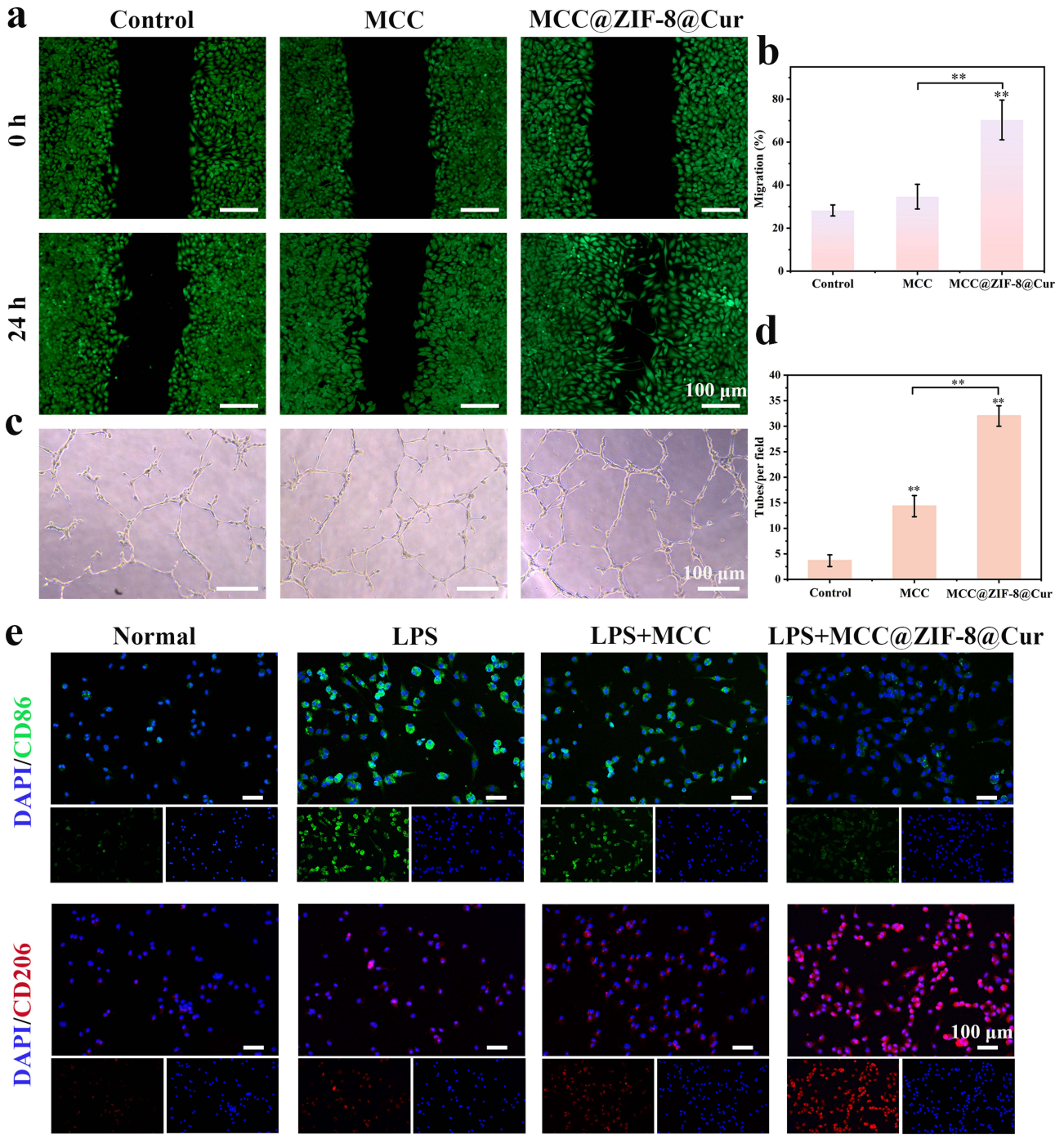

Figure 6 (**a**) Images of the scratch test in vitro. (**b**) Quantifiable data on migration within various groups. (**c**) Images of the development of tubes. (**d**) Quantifiable statistics for each field and tube in several groups. (**e**) Representative immunofluorescence images of CD86 and CD206 on the polarization of macrophages cocultured with hydrogels. Significance levels of $^{**}p<0.01$ were applied.

of 97.22% at 14th day, exhibited a markedly enhanced healing ratio ($p<0.001$) compared to both the Control group and the MCC hydrogel treatment group, demonstrating the most superior therapeutic efficacy.

Following 14 days of treatment, wound specimens underwent hematoxylin and eosin (H&E) testing, which revealed histologically significant wound healing. As illustrated in Figure 7c, the Control group exhibited abnormally thickened newly formed epithelium at the wound margins, disorganized basal layer cell arrangement, and a significant presence of inflammatory cells. The MCC hydrogel group showed improvement, while the MCC@ZIF-8@Cur hydrogel group displayed smoother, flatter epithelium with a more complete epithelial and dermal structure and reduced inflammatory

https://doi.org/10.2147/IJN.S505918

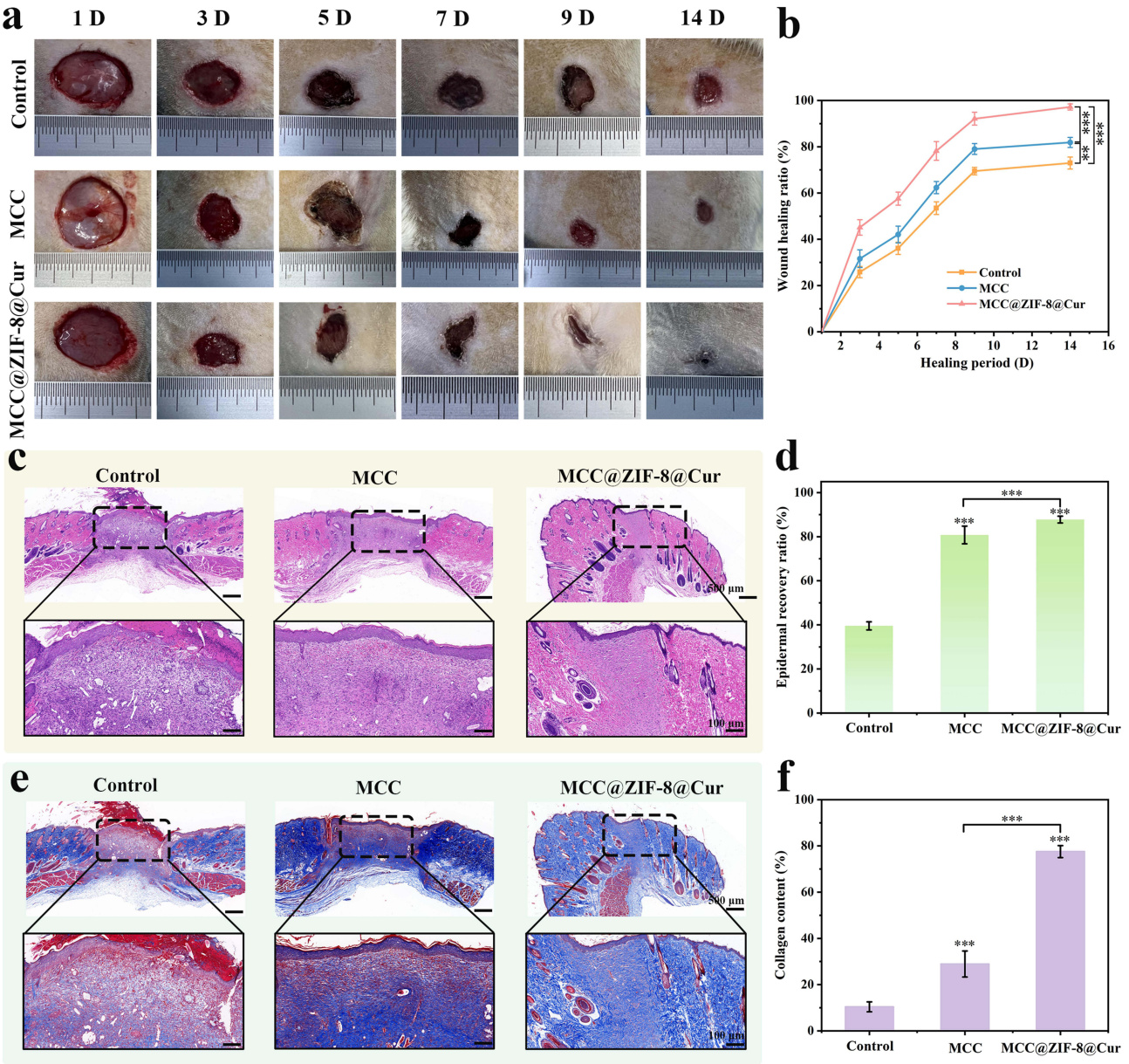

Figure 7 (**a**) pictures taken with digital devices of skin wounds that were healed in 14 days using different hydrogels. (**b**) Ratio of wound closure in the 14 days following surgery. (**c**) Images of the H&E staining. (**d**) Quantitative statistical analysis of the 14-day epidermal recovery ratio in various groups. (**e**) Images of the Masson staining. (**f**) Quantitative statistical of collagen in various groups at 14 days. Significance levels of $^{**}p<0.01$, and $^{***}p<0.001$ were applied.

cell infiltration. Quantitative assessment of epidermal recovery ratio indicated (Figure 7d) that the MCC@ZIF-8@Cur hydrogel group achieved an 87.86% after 14 days. Masson staining provided a more specific reflection of collagen deposition in the newly formed skin tissue. On the 14th day of wound healing, according to Figure 7e and f, the MCC@ZIF-8@Cur hydrogel group demonstrated orderly collagen formation with the highest collagen deposition, whereas collagen formation in the Control and MCC hydrogel groups was relatively loose. The histological findings corroborate the visual wound healing process, indicating that the MCC@ZIF-8@Cur hydrogel could significantly facilitates epithelial remodeling, reduces scar formation, and promotes orderly collagen deposition compared to the Control group and the MCC hydrogel group ($p<0.001$), thereby enhancing wound healing.

Afterward, Immunohistochemical images of IL-10 and IL-6 (Figure 8a) were used to investigate the expression of factors related to inflammation in wound tissue. These images revealed a significant decrease in the expression of all inflammatory factors in the MCC@ZIF-8@Cur hydrogel group, suggesting that ZIF-8@Cur nanoparticles improved the

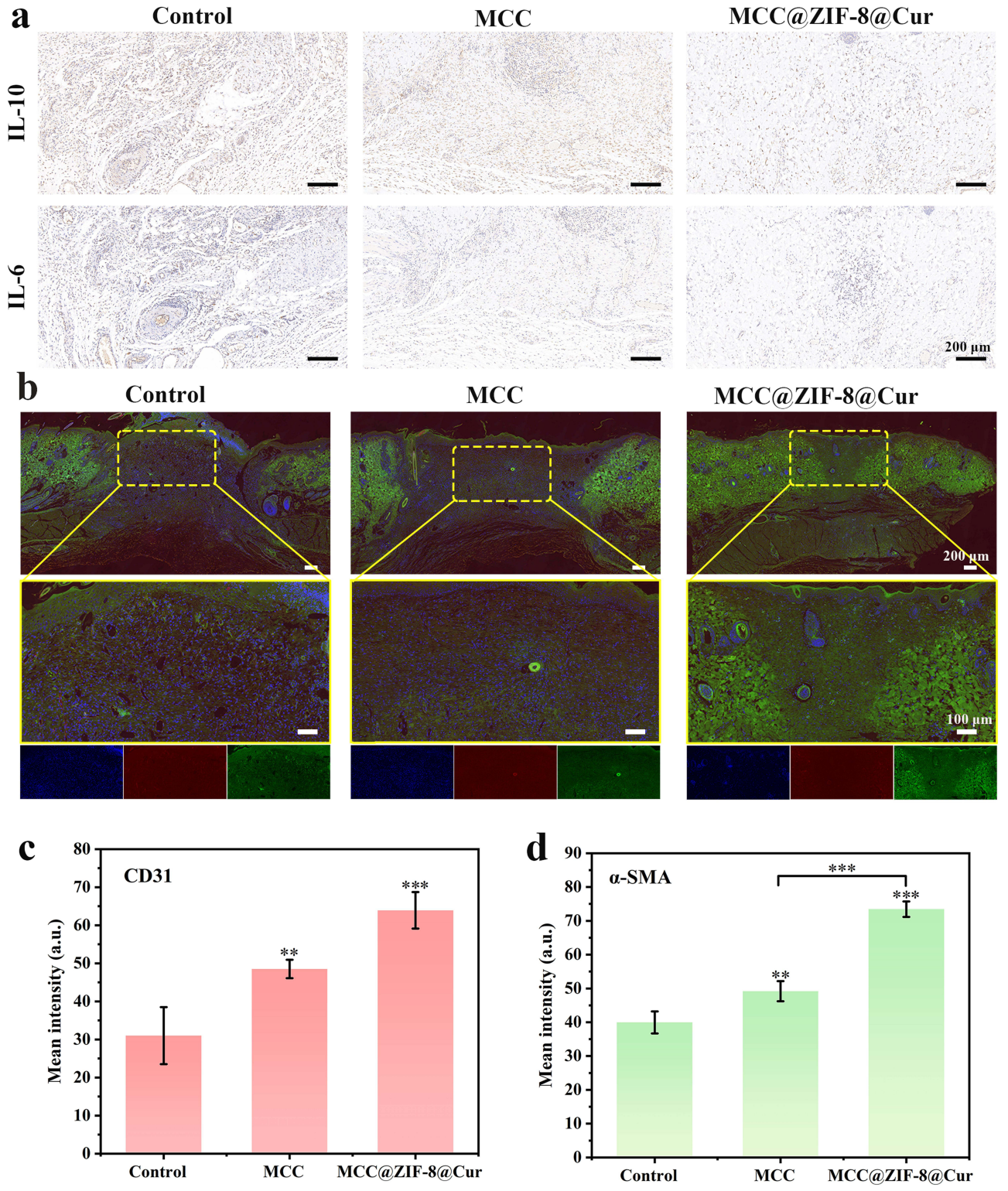

Figure 8 (**a**) Images of IL-10 or IL-6 immunohistochemistry staining. (**b**) Images of full-thickness wound α-SMA and CD31 immunohistochemistry staining after 14 days. (**c**) CD31's mean fluorescence intensity. (**d**) α-SMA's mean fluorescence intensity. Significance levels of $^{**}p<0.01$, and $^{***}p<0.001$ were applied.

chronic inflammatory response in DM wounds. Application of CD31 (red) and α-SMA (green) immunofluorescence labeling demonstrated the existence of neovascularization at different wound locations. According to the fluorescence images shown in Figure 8b and the quantitative analysis of fluorescence intensity for CD31 (Figure 8c) and α-SMA (Figure 8d), the MCC@ZIF-8@Cur hydrogel group exhibited higher fluorescence expression of CD31 and α-SMA. In

https://doi.org/10.2147/IJN.S505918

vivo measurement of blood vessel density is achieved by means of the vascular endothelium specific marker CD31.[48] while the expression of α-SMA indicates the presence of actin stress fibers, which are crucial for contraction and migration during wound healing.[49] This indicates even further that the MCC@ZIF-8@Cur hydrogel stimulates the development and expansion of myofibroblasts and endothelial cells. thereby facilitating angiogenesis and positively influencing tissue repair and fibrosis, ultimately enhancing wound healing.

In summary, the MCC@ZIF-8@Cur hydrogel, as an injectable thermosensitive hydrogel, can penetrate into deep wounds and accommodate irregular injuries. It provides excellent mechanical properties and a physical barrier, with moisture-retentive qualities and outstanding biocompatibility. The hydrogel matrix synergistically encapsulates Cur nanoparticles to exert functional effects that reduce the expression of inflammatory factors, mitigate inflammatory responses, enhance epithelial and vascular regeneration, diminish scar hyperplasia, and promote wound healing.

Conclusion

Chronic wounds associated with diabetes have long posed a formidable clinical challenge on a global scale. In this study, a temperature-sensitive hydrogel endowed with remarkable antibacterial and antioxidant properties was meticulously crafted. This hydrogel not only attenuates inflammatory responses but also modulates macrophage M2 polarization, fosters angiogenesis, and culminates in enhanced wound healing. The monomer of Chinese traditional herbs Cur, known for its potent anti-inflammatory capabilities, is efficiently loaded into ZIF-8 nanoparticles and combined with an MCC-based thermosensitive hydrogel matrix. The metal chelation between ZIF-8 and the hydrogel network, coupled with the physical interactions within the MCC double crosslinked network, shortens the gelation time of the MCC@ZIF-8@Cur hydrogel (475 s) and adjusts its gelation temperature (28 °C) to fall within the physiological temperature range. It is achieving the purpose of filling irregular wound deeply and the rapid formation of a physical barrier on the wound surface, guaranteeing the steady and continuous release of Zn^{2+} and Cur. Due to the pH-responsive of ZIF-8 in acidic environments, Cur is released in a controlled manner according to the real-time state of the wound, inhibits inflammation by controlling the polarization of macrophages to M2, which increases the production of anti-inflammatory factors. Additionally, the continuous breakdown of ZIF-8 releases Zn^{2+}, which further stimulates angiogenesis. After 14 days of treatment with the MCC@ZIF-8@Cur hydrogel, the wound healing ratio in rats reached 97.22%. Histological analysis confirmed that the MCC@ZIF-8@Cur hydrogel enhances epithelial regeneration, collagen deposition, angiogenesis, and fibroblast proliferation, leading to reduced healing time and improved remodeling and repair of wound tissue.

In a word, MCC@ZIF-8@Cur hydrogel with a wide range of raw materials, excellent biocompatibility and effective functionality have great application potential in promoting DM wounds. However, MCC@ZIF-8@Cur hydrogel has yet to undergo larger animal studies and human clinical trials. Future research will proceed to assess its safety and degradability through clinical trials and confirm its efficacy in real-world applications.

Acknowledgments

This work was supported by the Funding of Science and Technology Projects in Guangzhou (2024A03J1061), the Funding of Science and Technology Projects in Guangzhou (No. 202201020476), the Funding of Science and Technology Projects in Guangzhou (No. SL2022A04J01940), and the Natural Science Foundation of China (No. 82202689).

Disclosure

The authors declare no competing interest.

References

1. Birkenfeld AL, Mohan V. Prediabetes remission for type 2 diabetes mellitus prevention. *Nat Rev Endocrinol*. 2024;20(8):441–442. doi:10.1038/s41574-024-00996-8
2. Taylor R. Understanding the cause of type 2 diabetes. *Lancet Diab Endocrinol*. 2024;12(9):664–673. doi:10.1016/S2213-8587(24)00157-8
3. Buch Pranali J, Chai Y, Goluch Edgar D. Treating polymicrobial infections in chronic diabetic wounds. *Clin Microbiol Rev*. 2019;32(2):1–18.
4. Chengwei W, Yihao L, Xiaoxiao Y, et al. In-situ forming hydrogel incorporated with reactive oxygen species responsive and antibacterial properties for diabetic infected chronic wound healing. *Chem Eng J*. 2022;450:138077. doi:10.1016/j.cej.2022.138077

5. Liu C, Lv M, Xu Q, et al. Chronological adaptive polyoxometalate-based hydrogel for diabetic chronic wounds through synchronous bacterial ferroptosis death and immunomodulation. *Nano Today*. 2024;58:102415. doi:10.1016/j.nantod.2024.102415
6. Lou D, Luo Y, Pang Q, Tan W-Q, Ma L. Gene-activated dermal equivalents to accelerate healing of diabetic chronic wounds by regulating inflammation and promoting angiogenesis. *Bioact Mater*. 2020;5(3):667–679. doi:10.1016/j.bioactmat.2020.04.018
7. Tu Z, Chen M, Wang M, et al. Engineering bioactive M2 macrophage-polarized anti-inflammatory, antioxidant, and antibacterial scaffolds for rapid angiogenesis and diabetic wound repair. *Adv Funct Mater*. 2021;31(30):2100924. doi:10.1002/adfm.202100924
8. Cao Y, Chen B, Liu Q, et al. Dissolvable microneedle-based wound dressing transdermally and continuously delivers anti-inflammatory and pro-angiogenic exosomes for diabetic wound treatment. *Bioact Mater*. 2024;42:32–51. doi:10.1016/j.bioactmat.2024.08.016
9. Yuan Y, Fan D, Shen S, Ma X. An M2 macrophage-polarized anti-inflammatory hydrogel combined with mild heat stimulation for regulating chronic inflammation and impaired angiogenesis of diabetic wounds. *Chem Eng J*. 2022;433:133859. doi:10.1016/j.cej.2021.133859
10. Zhao H, Huang J, Li Y, et al. ROS-scavenging hydrogel to promote healing of bacteria infected diabetic wounds. *Biomaterials*. 2020;258:120286. doi:10.1016/j.biomaterials.2020.120286
11. Rao S, Lin Y, Lin R, et al. Traditional Chinese medicine active ingredients-based selenium nanoparticles regulate antioxidant selenoproteins for spinal cord injury treatment. *J Nanobiotechnol*. 2022;20(1):278. doi:10.1186/s12951-022-01490-x
12. Tian X, Wang P, Li T, et al. Self-assembled natural phytochemicals for synergistically antibacterial application from the enlightenment of traditional Chinese medicine combination. *Acta Pharm Sin B*. 2020;10(9):1784–1795. doi:10.1016/j.apsb.2019.12.014
13. Wang X, Huo H, Cao L, et al. Curcumin-release antibacterial dressings with antioxidation and anti-inflammatory function for diabetic wound healing and glucose monitoring. *J Control Release*. 2025;378:153–169. doi:10.1016/j.jconrel.2024.12.012
14. Ding Y-W, Zhang Z-W, Cui X-Y, et al. ZnCur nanoparticle-enhanced multifunctional hydrogel platform: synergistic antibacterial and immunoregulatory effects for infected diabetic wound healing. *Chem Eng J*. 2025;503:158387. doi:10.1016/j.cej.2024.158387
15. Ni S, Zhang K, Zhao X, et al. Phenylboronic acid functionalized dextran loading curcumin as nano-therapeutics for promoting the bacteria-infected diabetic wound healing. *Int J Biol Macromol*. 2024;273:133062. doi:10.1016/j.ijbiomac.2024.133062
16. Chen L-H, Chen T, Zhao R-N, et al. Physical properties and antioxidant activity of curcumin-zinc metal-organic frameworks. *Food Chem*. 2024;460:140449. doi:10.1016/j.foodchem.2024.140449
17. Xu H, Ma Q, Qiu C, et al. Encapsulation and controlled delivery of curcumin by self-assembled cyclodextrin succinate/chitosan nanoparticles. *Food Hydrocoll*. 2024;157:110465. doi:10.1016/j.foodhyd.2024.110465
18. Wang F, Sun M, Li D, et al. Multifunctional asymmetric bacterial cellulose membrane with enhanced anti-bacterial and anti-inflammatory activities for promoting infected wound healing. *Small*. 2023;19(48):2303591. doi:10.1002/smll.202303591
19. Fan Y-L, Liu H-J, Wang Z-L, et al. A one-nano MOF-two-functions strategy toward self-healing, anti-inflammatory, and antibacterial hydrogels for infected wound repair. *Chem Eng J*. 2024;497:155037. doi:10.1016/j.cej.2024.155037
20. Zhang X, Chen J, Pei X, et al. Drug-loading ZIF-8 for modification of microporous bone scaffold to promote vascularized bone regeneration. *Chin Chem Lett*. 2024;35(6):108889. doi:10.1016/j.cclet.2023.108889
21. Zhang X, Chen J-Y, Pei X, et al. One-pot facile encapsulation of dimethyloxallyl glycine by nanoscale zeolitic imidazolate frameworks-8 for enhancing vascularized bone regeneration. *Adv Healthcare Mater*. 2023;12(4):2202317. doi:10.1002/adhm.202202317
22. Wu J, Niu L, Yang K, et al. The role and mechanism of RNA-binding proteins in bone metabolism and osteoporosis. *Ageing Res Rev*. 2024;96:102234. doi:10.1016/j.arr.2024.102234
23. Gong J, Wang H, Xie C, et al. A multifunctional injectable hydrogel for boosted diabetic wound healing assisted by Quercetin-ZIF system. *Chem Eng J*. 2024;495:153425. doi:10.1016/j.cej.2024.153425
24. Wu R, Pang S, Lv W, et al. Injectable pH-responsive CI1040 delayed-release hydrogel for the treatment of tendon adhesion. *Adv Funct Mater*. 2024;34(30):2314731. doi:10.1002/adfm.202314731
25. Pang S, Wu R, Lv W, et al. Use of a pH-responsive imatinib mesylate sustained-release hydrogel for the treatment of tendon adhesion by inhibiting PDGFRβ/CLDN1 pathway. *Bioact Mater*. 2024;38:124–136. doi:10.1016/j.bioactmat.2024.04.012
26. Liu Y, Li T, Sun M, et al. ZIF-8 modified multifunctional injectable photopolymerizable GelMA hydrogel for the treatment of periodontitis. *Acta Biomater*. 2022;146:37–48. doi:10.1016/j.actbio.2022.03.046
27. Liu Y, Zhu Z, Pei X, et al. ZIF-8-modified multifunctional bone-adhesive hydrogels promoting angiogenesis and osteogenesis for bone regeneration. *ACS Appl Mater Interfaces*. 2020;12(33):36978–36995. doi:10.1021/acsami.0c12090
28. Jiang Y, Liao H, Yan L, et al. A metal–organic framework-incorporated hydrogel for delivery of immunomodulatory neobavaisoflavone to promote cartilage regeneration in osteoarthritis. *ACS Appl Mater Interfaces*. 2023;15(40):46598–46612. doi:10.1021/acsami.3c06706
29. Wang L, Li A, Zhang D, et al. Injectable double-network hydrogel for corneal repair. *Chem Eng J*. 2023;455:140698. doi:10.1016/j.cej.2022.140698
30. Zhang W, Song S, Huang J, Zhang Z. An injectable, robust double network adhesive hydrogel for efficient, real-time hemostatic sealing. *Chem Eng J*. 2023;476:146244. doi:10.1016/j.cej.2023.146244
31. Liu X, Ding Q, Liu W, et al. A Poloxamer 407/chitosan-based thermosensitive hydrogel dressing for diabetic wound healing via oxygen production and dihydromyricetin release. *Int J Biol Macromol*. 2024;263:130256. doi:10.1016/j.ijbiomac.2024.130256
32. Xie H, Wang Z, Wang R, et al. Self-healing, injectable hydrogel dressing for monitoring and therapy of diabetic wound. *Adv Funct Mater*. 2024;34(36):2401209. doi:10.1002/adfm.202401209
33. Yao S, Zhao Y, Xu Y, et al. Injectable dual-dynamic-bond cross-linked hydrogel for highly efficient infected diabetic wound healing. *Adv Healthc Mater*. 2022;11(14):2200516. doi:10.1002/adhm.202200516
34. Geng C, Liu X, Ma J, et al. High strength, controlled release of curcumin-loaded ZIF-8/chitosan/zein film with excellence gas barrier and antibacterial activity for litchi preservation. *Carbohydr Polym*. 2023;306:120612. doi:10.1016/j.carbpol.2023.120612
35. Wang M, Wang C, Chen M, et al. Efficient angiogenesis-based diabetic wound healing/skin reconstruction through bioactive antibacterial adhesive ultraviolet shielding nanodressing with exosome release. *ACS Nano*. 2019;13(9):10279–10293. doi:10.1021/acsnano.9b03656
36. Huang L, Li W, Guo M, et al. Silver doped-silica nanoparticles reinforced poly (ethylene glycol) diacrylate/hyaluronic acid hydrogel dressings for synergistically accelerating bacterial-infected wound healing. *Carbohydr Polym*. 2023;304:120450. doi:10.1016/j.carbpol.2022.120450
37. Feng Y, Qin S, Yang Y, et al. A functional hydrogel of dopamine-modified gelatin with photothermal properties for enhancing infected wound healing. *Colloids Surf B Biointerfaces*. 2024;241:114058. doi:10.1016/j.colsurfb.2024.114058

38. Jian X, Wang H, Jian X, et al. A flexible adhesive hydrogel dressing of embedded structure with pro-angiogenesis activity for wound repair at moving parts inspired by commercial adhesive bandages. *Matre Today Adv*. 2024;21:100452. doi:10.1016/j.mtadv.2023.100452
39. Wei J, Duan D, Jing Y, et al. Heparin-conjugated injectable hydrogels with sustained releasing capability for promotion of H-type vessels formation and rat femoral bone defects repair. *Mater Des*. 2023;235:112407. doi:10.1016/j.matdes.2023.112407
40. Liang W, Xie Z, Cheng J, et al. A light-triggered pH-responsive metal–organic framework for smart delivery of fungicide to control sclerotinia diseases of oilseed rape. *ACS Nano*. 2021;15(4):6987–6997. doi:10.1021/acsnano.0c10877
41. Zhu M, Hu X, Liu H, et al. Antibacterial peptide encapsulation and sustained release from chitosan-based delivery system. *Eur Polym J*. 2022;181:111640. doi:10.1016/j.eurpolymj.2022.111640
42. Sun H, Xu J, Wang Y, et al. Bone microenvironment regulative hydrogels with ROS scavenging and prolonged oxygen-generating for enhancing bone repair. *Bioact Mater*. 2023;24:477–496. doi:10.1016/j.bioactmat.2022.12.021
43. Shao N, Huang S, Huang Y, et al. Smart enzyme-like polyphenol-copper spray for enhanced bacteria-infected diabetic wound healing. *Small*. 2024;20(22):2308295. doi:10.1002/smll.202308295
44. Taheri M, Ashok D, Sen T, et al. Stability of ZIF-8 nanopowders in bacterial culture media and its implication for antibacterial properties. *Chem Eng J*. 2021;413:127511. doi:10.1016/j.cej.2020.127511
45. Yu Z, Li M, Yang L, et al. Enhancing diabetic wound healing: a two-pronged approach with ROS scavenging and ROS-independent antibacterial properties. *Nano Today*. 2024;57:102358. doi:10.1016/j.nantod.2024.102358
46. Shao Z, Yin T, Jiang J, et al. Wound microenvironment self-adaptive hydrogel with efficient angiogenesis for promoting diabetic wound healing. *Bioact Mater*. 2023;20:561–573. doi:10.1016/j.bioactmat.2022.06.018
47. Zhu S, Dai Q, Yao L, et al. Engineered multifunctional nanocomposite hydrogel dressing to promote vascularization and anti-inflammation by sustained releasing of Mg2+ for diabetic wounds. *Compos Part B- Eng*. 2022;231:109569. doi:10.1016/j.compositesb.2021.109569
48. Liu H, Qin S, Zhang H, et al. Silk sericin-based ROS-responsive oxygen generating microneedle platform promotes angiogenesis and decreases inflammation for scarless diabetic wound healing. *Adv Funct Mater*. 2024;2024:2404461.
49. Zong L, Teng R, Zhang H, et al. Ultrasound-responsive HBD peptide hydrogel with antibiofilm capability for fast diabetic wound healing. *Adv Sci*. 2024;11(42):2406022. doi:10.1002/advs.202406022